Physics Letters B ••• (••••) ••••••

ELSEVIER

Contents lists available at ScienceDirect

Physics Letters B

www.elsevier.com/locate/physletb



Jet charge: A new tool to probe the anomalous $Zb\bar{b}$ couplings at the EIC

Hai Tao Li^a, Bin Yan^b, C.-P. Yuan^c

- a School of Physics, Shandong University, Jinan, Shandong 250100, China
- b Theoretical Division, Group T-2, MS B283, Los Alamos National Laboratory, P.O. Box 1663, Los Alamos, NM 87545, USA
- ^c Department of Physics and Astronomy, Michigan State University, East Lansing, MI 48824, USA

ARTICLE INFO

Article history: Received 23 December 2021 Received in revised form 30 May 2022 Accepted 8 July 2022 Available online xxxx Editor: G.F. Giudice

ABSTRACT

We propose to probe the $Zb\bar{b}$ interactions at the Electron-Ion Collider (EIC) by utilizing the average jet charge weighted single-spin asymmetry A_e^{bQ} , which is induced by different cross sections of a left-handed and right-handed electron beam scattering off an unpolarized proton beam in the neutral current deeply-inelastic scattering processes with one observed b-tagged jet. This novel observable at the EIC is sensitive to the axial-vector component of the $Zb\bar{b}$ coupling, providing similar information as the $gg \rightarrow Zh$ cross section measurement at the high-luminosity Large Hadron Collider, and is complementary to the single-spin asymmetry measurement at the EIC which is sensitive to the vector component of the $Zb\bar{b}$ coupling. We show that the apparent degeneracy of the allowed $Zb\bar{b}$ coupling in its vector and axial-vector components, implied by the Large Electron-Positron Collider (LEP) and the Stanford Linear Collider (SLC) precision electroweak data, can be broken by the A_e^{bQ} measurement at the EIC. With a large enough integrated luminosity collected at the EIC, the measurement of A_e^{bQ} could also resolve the long-standing discrepancy between bottom quark forward-backward asymmetry $A_{\rm FB}^b$ at the LEP and the Standard Model prediction, with a strong dependence on the b-tagging efficiency.

© 2022 Published by Elsevier B.V. This is an open access article under the CC BY license (http://creativecommons.org/licenses/by/4.0/). Funded by SCOAP³.

1. Introduction

The electroweak precision measurements at the Large Electron-Positron collider (LEP) and the Stanford Linear Collider (SLC) play a crucial role to test the Standard Model (SM) and beyond. An interesting observation at the LEP is that the bottom quark forwardbackward asymmetry (A_{FR}^b) , i.e., an asymmetry in the production cross sections of bottom quark traveling along or against the electron beam direction, at the Z-pole exhibits a long-standing discrepancy with the SM prediction, with a significance around 2.1σ [1]. Such a startling deviation has been received much attention in the high energy physics community, and consequently, many new physics (NP) models have been proposed in the literature to explain the LEP data [2-5]. A well known example is that the model with an underlying approximate custodial symmetry, which introduces a sizable right-handed Zbb coupling, while keeping the left-hand Zbb coupling about the same as the SM prediction [3]. Such theory can not only explain the anomaly of A_{FR}^b , but also satisfy the limits from the R_b and A_b measurements at

the Z-pole. Here, the R_b is defined as the branching fraction of $Z \to b\bar{b}$ to the inclusive hadronic decay of the Z boson at LEP and A_b is the left-right forward-backward asymmetry of b production at the SLC.

However, the $Zb\bar{b}$ couplings can not be fully determined by the global analysis of the LEP and SLC data. It has been shown that there are two possible solutions in the parameter space of Zbb vector and axial-vector couplings, after combining the A_b , R_b and $A_{\rm FR}^b$ measurements at the Z-pole and off Z-pole [2]. Breaking the above-mentioned degeneracy and further pinning down the coupling strength as well as confirming or excluding the anomaly of A_{FB} measurement at the LEP is one of the major tasks of the particle physics at the current and future colliders. Recently, we demonstrated that the axial-vector component of Zbb coupling can be determined by the precision measurement of $gg \rightarrow Zh$ production at the Large Hadron Collider (LHC) and the high-luminosity LHC (HL-LHC) [6], while its vector component can be better constrained by the measurement of single-spin asymmetry (SSA) in the polarized lepton-hadron collisions, such as at HERA and the upcoming Electron-Ion Collider (EIC) [7].

It was concluded in [7] that the SSA at the EIC is only sensitive to the vector component of the $Zb\bar{b}$ coupling. To probe its

https://doi.org/10.1016/j.physletb.2022.137300

0370-2693/© 2022 Published by Elsevier B.V. This is an open access article under the CC BY license (http://creativecommons.org/licenses/by/4.0/). Funded by SCOAP3.

E-mail addresses: haitao.li@sdu.edu.cn (H.T. Li), binyan@lanl.gov (B. Yan), yuan@pa.msu.edu (C.-P. Yuan).

Physics Letters B ••• (••••) •••••

axial-vector component at the EIC calls for a novel idea, that is to measure the average jet charge weighted single-spin asymmetry (WSSA) of the polarized electron-proton cross section in neutral current deeply-inelastic scattering (DIS) processes with one b-tagged jet in the final state. The WSSA, A_e^{bQ} , is defined as

$$A_e^{bQ} = \frac{\sigma_{b,+}^{Q} - \sigma_{b,-}^{Q}}{\sigma_{b,+}^{Q} + \sigma_{b,-}^{Q}},\tag{1}$$

where $\sigma_{b,\pm}^{\mathbb{Q}}$ is the average jet charge weighted total inclusive b-tagged DIS cross section of a right-handed (+) or left-handed (-) electron beam scattering off an unpolarized proton (p) beam, *i.e.*,

$$\sigma_{b,\pm}^{\mathcal{Q}} = \int dp_T^j \frac{d\sigma_{b,\pm}^{\text{tot}}}{dp_T^j} \langle \mathcal{Q}_J \rangle_b(p_T^j). \tag{2}$$

Here, $(Q_J)_b(p_T^J)$ is the average jet charge of a *b*-tagged jet with transverse momentum p_T^j , and can be written as

$$\langle Q_J \rangle_b(p_T^j) = \sum_{q=u.d.c.s.b} \left[f_J^q(p_T^j, \epsilon_q^b) - f_J^{\bar{q}}(p_T^j, \epsilon_q^b) \right] \langle Q_J^q \rangle(p_T^j). \quad (3)$$

Here, $\langle Q_J^q \rangle$ is the average jet charge of the q-type jet, and f_J^q represents the fraction of the q-type jets which have been (mis) tagged as the b-tagged jets in the final state. f_J^q depends on the tagged jet p_T^j and ϵ_q^b which is the efficiency of (mis-)tagging a q-jet as a b-jet. The minus sign in Eq. (3) is because of the opposite electric charge of quark and its anti-quark. It has been demonstrated that the jet charge can be used to separate the quark jets from anti-quark jets and to tag the flavor of the quark jets [8–13], and has been measured by both the ATLAS and CMS Collaborations [14,15]. In this work, we propose to measure the b-tagged jet charge to probe the $Zb\bar{b}$ coupling at the polarized electron-hadron colliders.

A detailed analysis on how the anomalous Zbb coupling could affect the value of SSA has been presented in Ref. [7]. It showed that the SSA (by setting $\langle Q_I \rangle_b = 1$ in Eq. (2)) depends linearly on the vector component of the $Zb\bar{b}$ coupling through the $\gamma - Z$ interference diagram, while the term linearly proportional to the axialvector component is associated with the F_3 structure function, which involves the convolution of the difference between quark and anti-quark parton distribution functions (PDFs), $(f_q - f_{\bar{q}})$. Since bottom (q = b) PDF is generated perturbatively through DGLAP evolution [16,17], $(f_b - f_{\bar{b}})$ must be zero at the leading-order (LO) and next-to-leading order (NLO), though it can be non-vanishing at the NNLO [7]. That explains why the SSA is only sensitive to the vector component of the Zbb coupling. In contrast, the WSSA is expected to be sensitive to its axial-vector component. This is due to the insertion of the average jet charge $(Q_I)_b$, which depends on the difference between quark and anti-quark cross sections, in the weighted cross section $\sigma_{b,\pm}^Q$, cf. Eq. (2). Below, we detail our analysis to demonstrate that the measurement of WSSA can be used to constrain the axial-vector Zbb coupling at the EIC, and provide complementary information to the measurements of the $gg \rightarrow Zh$ production cross section at the HL-LHC and the SSA at the EIC.

2. The jet charge

The jet charge is defined as the transverse momentum-weighted sum of the charges of the jet constituents [18],

$$Q_J = \frac{1}{\left(p_T^j\right)^{\kappa}} \sum_{i \in \text{jet}} Q_i(p_T^i)^{\kappa}, \ \kappa > 0, \tag{4}$$

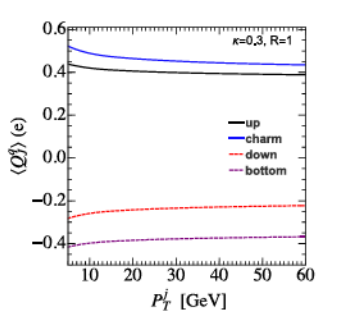


Fig. 1. The average jet charge distributions (Q_J^q) for various quark-type jets as a function of jet p_T^j , with $\kappa=0.3$. Here, the jet size R=1 and the factorization scale $\mu=p_T^jR$.

where p_T^i and Q_i are the transverse momentum and electric charge of particle i, respectively. Based on the soft-collinear effective theory [19–22], the average of the jet charge of a quark (q) jet is found to be [8,9]

$$\langle Q_{J}^{q} \rangle = \frac{\widetilde{J}_{qq}(p_{T}^{j}, R, \kappa, \mu)}{J_{q}(p_{T}^{j}, R, \mu)} \widetilde{D}_{q}^{Q}(\kappa) \times \exp \left[\int_{0}^{\mu} \frac{d\mu'}{\mu'} \frac{\alpha_{s}(\mu')}{\pi} \widetilde{f}_{q \to qg}(\kappa) \right], \tag{5}$$

where R and μ are jet size and factorization scale, respectively. $J_q(p_T^j,R,\mu)$ is a jet function and $\widetilde{J}_{qq}(p_T^j,R,\kappa,\mu)$ is the $(\kappa+1)$ -th Mellin moment of the Wilson coefficient for matching the quark fragmenting jet function onto a quark fragmentation function. The NLO calculation of J_q and \widetilde{J}_{qq} can be found in Refs. [9,23,24]. $\widehat{f}_{q\to qg}(\kappa)$ is the $(\kappa+1)$ -th Mellin moment of the splitting function $f_{q\to qg}(z)$. The initial scale of the evolution of fragmentation function is set to $\mu_0=1$ GeV for light jets and $\mu_0=m_Q$ for heavy flavor jets. Here, m_Q is taken to be the pole mass of the heavy flavor quark. The only non-perturbative parameter $\widetilde{D}_q^Q(\kappa)$ depends on the parameter κ and the flavor of jet, which can be written as $\widetilde{D}_q^Q(\kappa)=\sum_h Q_h\int_0^1 dxx^\kappa D_q^h(\kappa,\mu_0)$. In this work, they are obtained from PYTHIA simulations [25]. Note that the non-perturbative parameter in Eq. (5) is independent of the jet p_T^j and jet size R.

The average jet charge distribution of various quark jets is depicted in Fig. 1, as a function of jet p_T^j with $\kappa=0.3$, R=1 and the factorization scale set to be $\mu=p_T^jR$. It shows that the sign of the jet charge is consistent with the sign of the electric charge of the parent parton. Furthermore, $\langle Q_J^q \rangle$ is not very sensitive to p_T^j , and approaches to a constant value as p_T^j increases. For the heavy flavor jet, because the initial scale μ_0 is larger and the fragmentation function $D_Q^h(z,\mu_0)$ has a much larger value in the large z region [26], the average jet charge for charm (c) or bottom (b) jet is larger than the ones for light flavor jets.

3. DIS cross section

Next, we consider the impact of the non-standard $Zb\bar{b}$ couplings to the WSSA A_e^{bQ} in Eq. (1) at the EIC. The $Zb\bar{b}$ effective Lagrangian can be parametrized as

$$\mathcal{L}_{\text{eff}} = \frac{g_W}{2c_W} \bar{b} \gamma_\mu (\kappa_V g_V^b - \kappa_A g_A^b \gamma_5) b Z_\mu, \tag{6}$$

where g_W is the electroweak gauge coupling and c_W is the cosine of the weak mixing angle θ_W . The couplings $g_V^b = -1/2 + 2/3s_W^2$ and $g_A^b = -1/2$ with $s_W \equiv \sin\theta_W$ are the vector and axial-vector

70

71

72

73

74

75

76

77

78

79

80

81

82

84

85

87 88

89

90

91

92

93

94

95

96

97

98

99

100

101 102

103

104

105

106

107

108

109

110

111

112

113

114

115

116

117

118

119

120

121

122

123

124

125

126

127

128

129

130

131

10

11

12

13

14

15

16

17

18

19

20

21

22

23

24

25

26

27

28

29

30

31

32

33

34

35

36

37

38

39

40

41

42

43

45

46

47

48

49

50

51

52

53

54

55

56

57

58

59

60

65

66

Physics Letters B ••• (••••) •••••

components of the Zbb coupling in the SM, respectively. We introduce the parameters $\kappa_{V,A}$ to include the possible NP effects for the $Zb\bar{b}$ interactions, and $\kappa_{V,A}=1$ in the SM.

To probe the $Zb\bar{b}$ coupling using the WSSA measurement, a final state b-jet needed to be tagged in the DIS production. As shown in Eq. (3), the average jet charge of a b-tagged jet, $(Q_J)_b(p_T^J)$, depends on the efficiency (ϵ_q^b) of (mis-)tagging a q-jet as a b-jet. In this study, we adopt two sets of benchmark tagging efficiencies [7] as

$$\begin{aligned} (i) \ \epsilon_q^b &= 0.001, & \epsilon_c^b &= 0.03, & \epsilon_b^b &= 0.7; \\ (ii) \ \epsilon_a^b &= 0.01, & \epsilon_c^b &= 0.2, & \epsilon_b^b &= 0.5, \end{aligned} \tag{7}$$

where q = u, d, s denotes the light quarks. The scenario (i) represents a good b-tagging efficiency, and (ii) a worse one. After combining all possible quark flavor contributions, the b-tagged differential distribution can be approximated at the LO as

$$\frac{d\sigma_{b,\pm}^{\text{tot}}}{dp_J^j} = \sum_{q=u,d,s} \frac{d\sigma_{q,\pm}}{dp_J^j} \epsilon_q^b + \frac{d\sigma_{c,\pm}}{dp_J^j} \epsilon_c^b + \frac{d\sigma_{b,\pm}}{dp_J^j} (\kappa_V, \kappa_A) \epsilon_b^b. \tag{8}$$

We will follow Ref. [10] and approximate the NLO inclusive jet cross section in the lepton-hadron collision as the product of the differential cross section of the production process $d\sigma_q(P_e, \mu_R, \mu_F)/dp_T^J$ evaluated at the LO and the jet function (J_a) at the NLO. This approximation holds in the narrow-jet approximation when the needed matching coefficient is also calculated at the NLO, as explicitly shown in Ref. [10]. In our numerical calculation, we have set the energy of the electron (E_e) and proton (E_p) beams to be 18 GeV and 275 GeV, respectively. Both the renormalization and factorization scales are fixed at $\mu_R = \mu_F = \sqrt{Q^2 + (p_T^j)^2}$, where $Q = \sqrt{-q^2}$ with q^μ being the momentum transfer of the electrons. We have also required the final state jet (with jet size R = 1) pass the following kinematical cuts: $p_T^j > 5$ GeV and $-2 < \eta_j < 4$, where η_j is the rapidity of jet measured in the lab frame. To calculate the heavy flavor contributions, such as the charm and bottom quarks, we adopt the sACOT- χ scheme [27-31]. At the LO, this amounts to setting its mass (m) to be zero in calculating the scattering amplitude, while replacing the momentum fraction (Bjorken x) carried by the heavy parton by $\chi = x(1 + 4m^2/Q^2)$ [31]. Here, we use $m_c = 1.3$ GeV and $m_h = 4.75$ GeV, to be consistent with the CT14LO parton distribution functions (PDFs) [32] adopted in this work, The strong coupling constant is taken to be $\alpha_s(M_Z) = 0.118$ at the Z boson mass scale.

Below, we give a detailed analysis of the dependence of A_e^{bQ} on the κ_V and κ_A parameters. As shown in Ref. [7], κ_V and κ_A can contribute to the b-tagged SSA through $g_A^e \cdot \kappa_V$ or $g_V^e \cdot \kappa_A$ in the γZ interference diagram, and $\left((g_V^e)^2+(g_A^e)^2\right)\cdot\kappa_V\kappa_A$ or $g_V^e g_A^e \cdot (\kappa_V^2 + \kappa_A^2)$ in the Z-only diagram, where $g_{V,A}^e$ are the vector and axial-vector components of the Zee couplings. However, the contributions from $g_V^e \cdot \kappa_A$ and $\kappa_V \kappa_A$ are associated with the F_3 structure function, which involves the convolution of $(f_b - f_{\bar{b}})$, and must be vanishing at the LO and NLO, for the bottom quark PDF is generated perturbatively through DGLAP evolution [16,17]. Hence, up to the NLO, only the terms proportional to $g_A^e \cdot \kappa_V$ and $(\kappa_V^2 + \kappa_A^2)$ will contribute to the *b*-tagged SSA. On the other hand, the jet charged weighted cross section $\sigma_{b,\pm}^Q$ is weighted by the electric charge of Q, cf. Eq. (2), as compared to the cross section $\sigma_{b,\pm}^{\mathrm{tot}}$ used in the calculation of SSA. Hence, on the contrary, the contributions from $g_A^e \cdot \kappa_V$ and $(\kappa_V^2 + \kappa_A^2)$ in WSSA will be vanishing, and only the terms proportional to $g_V^e \cdot \kappa_A$ and $\kappa_V \kappa_A$ will contribute to the *b*-tagged WSSA. Since the *Z*-only diagram will be suppressed by one more power of Z propagator, we expect the

WSSA would dominantly depend linearly on κ_A through the γZ interference diagram. Another important difference between WSSA and SSA is that the contribution from the Z-only diagram ($\kappa_V \kappa_A$ term) cannot be ignored in WSSA, because $g_V^e \ll g_A^e$. Similar to the SSA, the y-only diagram will not change the conclusion and only contribute to the denominator of the WSSA.

4. Sensitivity at the EIC

Below, we consider the WSSA measurement at the upcoming EIC with polarized electron beam. For simplicity, we assume that both the right- and left-handed electron beams have the same degree of polarization, with the same integrated luminosity. The WSSA in Eq. (1) can be related to the experimental observable as

$$A_e^{bQ} = \frac{1}{P_e} \frac{\sigma_b^Q(P_e) - \sigma_b^Q(-P_e)}{\sigma_b^Q(P_e) + \sigma_b^Q(-P_e)},\tag{9}$$

where $\sigma_b^Q(P_e)$ denotes the average jet charge weighted b-tagged cross section in the experiment for the electron beam with polarization $P_e = 70\%$ at the EIC [33], and it can be related to the cross sections with the incoming electron at its helicity eigenstates as,

$$\sigma_b^Q(P_e) = \frac{1}{2} \left(\sigma_{b,+}^Q + \sigma_{b,-}^Q \right) + \frac{P_e}{2} \left(\sigma_{b,+}^Q - \sigma_{b,-}^Q \right). \tag{10}$$

With the considered tagging efficiencies in Eq. (7) and the degree of polarization of the electron beam at the EIC, we calculate various (anti-)quark fraction distributions f_{i}^{q} , which is defined as:

$$f_{j}^{q}(p_{T}^{j}, \epsilon_{q}^{b}) \equiv \left(\frac{d\sigma_{q}}{dp_{T}^{j}} \epsilon_{q}^{b}\right) / \left(\frac{d\sigma_{b}^{\text{tot}}}{dp_{T}^{j}}\right), \tag{11}$$

where the differential cross section $d\sigma_q(P_e, \mu_R, \mu_F)/dp_T^J$, cf. Eq. (8), can be written as a convolution of the PDFs and partonic cross section according to the collinear factorization theorem. Note that both the down and strange (anti-)quark contributions have been added in f_I^d and f_I^d , for simplicity. With the result depicted in Fig. 2, several comments are in order:

- The fractions $f_J^{u(d)} \gg f_J^{\bar{u}(\bar{d})}$, while $f_J^{c(b)} \sim f_J^{\bar{c}(\bar{b})}$, because the up and down quarks contain both the valence and sea quarks (with $u_{seq} = \bar{u}$, etc.), while the charm and bottom quarks are sea quarks.
- ullet We notice a small difference between $f_J^{c(b)}$ and $f_J^{ar c(ar b)}$ in the high p_T^j region. It arises from the fact that the axial-vector Zqar qcoupling yields an opposite contribution from quark and antiquark scattering processes [7]. The difference becomes obvious only when the interference effect induced by the γZ diagram leads to a sizable contribution to the total cross section, i.e., in the high p_T^J region.
- The quark fraction distributions f_I^q are strongly dependent on the jet tagging efficiencies, because the cross sections of the light quarks are much larger than the bottom quark.
- The fractions $f_I^{b,b}$ are very sensitive to the bottom quark mass in the small p_T^j region due to the rescaling of the Bjorken x in the sACOT- χ scheme adopted in this calculation.

In Fig. 3, we show the total average jet charge distributions, cf. Eq. (3), with $\kappa = 0.3$ at the EIC. The red and blue curves denote the predictions with the tagging efficiency scenarios (i) and (ii) in Eq. (7), respectively. It shows that the expected $(Q_I)_h$ is sensitive to the jet tagging efficiencies and the heavy quark mass

H.T. Li, B. Yan and C.-P. Yuan

g

Physics Letters B ••• (••••) ••••

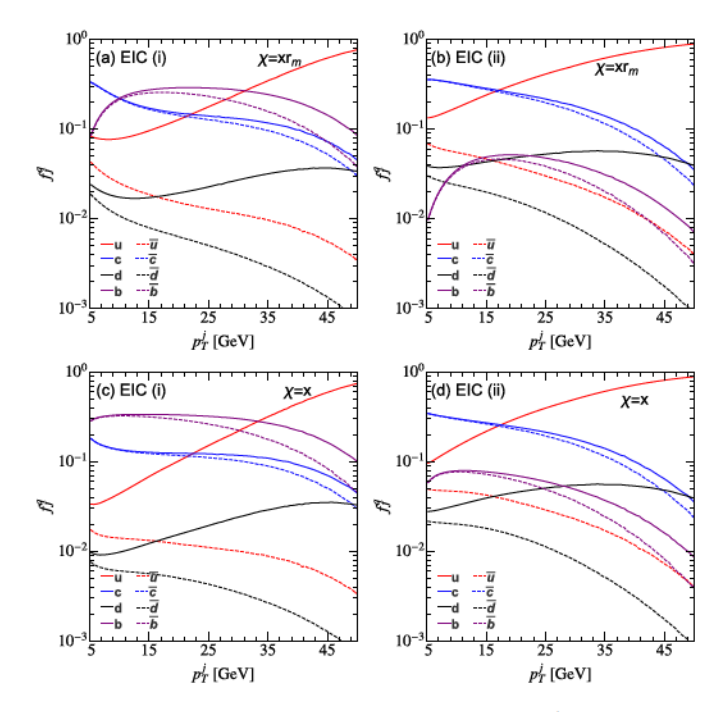


Fig. 2. The quark fraction distributions f_i^q as a function of jet p_T^j at the EIC, with the tagging efficiency scenarios (i) and (ii), cf. Eq. (7), respectively. Here, x is the Bjorken-x value, $r_m = 1 + 4m_{e,h}^2/Q^2$, and the electron beam polarization $P_e = 70\%$. Both the down and strange (anti-)quark contributions have been added in the d and

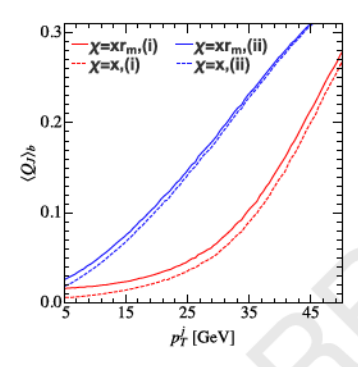


Fig. 3. The total average jet charge distribution of a b-tagged jet $(Q_I)_b$ as a function of jet p_T^J at the EIC. The red and blue curves correspond to the tagging efficiency scenarios (i) and (ii), cf. Eq. (7), respectively. Here, x is the Bjorken-x value, $r_m =$ $1 + 4m_{c,b}^2/Q^2$, and the electron beam polarization $P_e = 70\%$.

effects. Such behavior could be understood from the quark fraction distributions f_I^q in Fig. 2. The comparison of Figs. 2(c) and (d) shows that the fraction f_I^u is significantly enhanced with the tagging scenario (ii), as compared to (i), while this enhancement is suppressed after including the heavy quark mass effects via adopting the sACOT- χ scheme, cf. Figs. 2(a) and (b). Also, the behavior of $f_I^{b,\bar{b}}$ is different from that of f_I^u .

Below, we combine the differential distribution $d\sigma_{b,\pm}^{\rm tot}/dp_T^J$ and the total average jet charge to estimate the sensitivity of the WSSA to the Zbb anomalous couplings at the EIC. The systematic uncertainties are assumed to be canceled in the WSSA definition and will be ignored in this work [34]. With the tagging efficiencies (i) and (ii) in Eq. (7), we obtain the WSSA at the EIC,

(i)
$$A_e^{bQ} = \frac{10.3 - 13.0\kappa_A - 4.6\kappa_V \kappa_A}{-1073.9 + 117.2\kappa_A + \kappa_A \kappa_V},$$

(ii) $A_e^{bQ} = \frac{120.5 - 13.0\kappa_A - 4.6\kappa_V \kappa_A}{-14748.5 + 117.2\kappa_A + \kappa_A \kappa_V}.$ (12)

It shows that A_e^{bQ} only depends on the linear combination of κ_A and $\kappa_V \kappa_A$, as expected, with a larger coefficient associated with the former term. The statistical uncertainty of A_e^{bQ} could be well controlled due to the large DIS cross section, i.e. (i) $\sigma_b^{\text{tot}} = 77 \text{ pb}$ and (ii) $\sigma_b^{\text{tot}} = 417 \text{ pb}$. With the integrated luminosity $\mathcal{L}=100~{\rm fb^{-1}}$, the WSSA in the SM are (i) $A_e^{bQ}=0.008$, with $\delta A_e^{bQ}/A_e^{bQ}=5\%$; (ii) $A_e^{bQ}=-0.007$, with $\delta A_e^{bQ}/A_e^{bQ}=3\%$, where δA_e^{bQ} denotes the statistical uncertainty of A_e^{bQ} . We notice that $A_e^{b\bar{Q}}$ changes sign from the case with tagging efficiency (i) to (ii). It arises from the fact that the jet charge weighted cross sections of the non-b jets are highly enhanced when using a worse tagging efficiency, as specified in (ii).

In Fig. 4, we show the expected limits, at the 68% confidence level (C.L.), on the anomalous Zbb couplings for various integrated luminosities, obtained from the WSSA (purple and gray bands) and SSA (orange and green bands) measurements at the EIC. The blue and red bands denote the limits imposed by the R_b and (A_{FR}^b, A_b) measurements at the Z-pole, respectively. It is evident that the measurement of A_e^{bQ} (purple and gray bands) is more sensitive to the axial vector component of the Zbb coupling, i.e., κ_A , while the SSA (orange and green bands) is more sensitive to the vector component κ_V , cf. Ref. [7]. The shapes of the bands from WSSA are determined by the relative size of the γZ and Z-only diagrams and dominantly depend on the interference effect of the yZ diagram. We note that the WSSA and SSA have a different sensitivity to the Zbb couplings as compared to the measurement of $gg \rightarrow Zh$ scattering cross section at the LHC [6]. Therefore, the measurements of WSSA and SSA at the EIC provide complementary information on the Zbb couplings to the above-mentioned measurements conducted at the LHC and lepton colliders.

We could also derive the minimal amount of integrated luminosities needed to exclude the degeneracy parameter space, implied by the precision electroweak data, with $\kappa_{V,A} < 0$ at the 68% C.L. The results for the two choices of the tagging efficiencies (i and ii in Eq. (7)) are found to be (see Fig. 4(a))

(i):
$$\mathcal{L} > 0.03 \text{ fb}^{-1}$$
; (ii): $\mathcal{L} > 1.5 \text{ fb}^{-1}$. (13)

To resolve the apparent degeneracy in the parameter space with $\kappa_{V,A} > 0$, i.e., $(\kappa_V, \kappa_A) = (1.46, 0.67)$, the needed minimal luminosities are (see Fig. 4(b))

$$(i): \mathcal{L} > 0.6 \,\text{fb}^{-1}; \quad (ii): \mathcal{L} > 36.4 \,\text{fb}^{-1}.$$
 (14)

Finally, the minimal luminosities to exclude the LEP A_{FR}^b measurement (the solution which is close to the SM) through WSSA are (see Fig. 4(c))

(i):
$$\mathcal{L} > 122 \text{ fb}^{-1}$$
; (ii): $\mathcal{L} > 8583 \text{ fb}^{-1}$. (15)

Note that the constraint with the worse tagging efficiency (ii) is not plotted in Fig. 4(c), for the required luminosity to exclude the A_{FR}^{b} anomaly is too large. Although it would be challenging to verify or exclude the LEP A_{FR}^b measurement through WSSA with a worse tagging efficiency, such goal could be realized via SSA over a few years of running as shown in Ref. [7].

5. Conclusions

In this work, we propose a novel method to probe the Zbb anomalous couplings by measuring the average jet charge weighted single-spin asymmetry A_e^{bQ} , in the total inclusive btagged DIS cross section, of a polarized electron beam scattering off an unpolarized proton beam at the EIC. We show that both the quark fraction $f_I^q(p_T^j)$ and the average jet charge $\langle Q_J \rangle_b(p_T^j)$ distributions of a b-tagged jet are sensitive to the b-tagging efficiency

 Physics Letters B ••• (••••) •••••

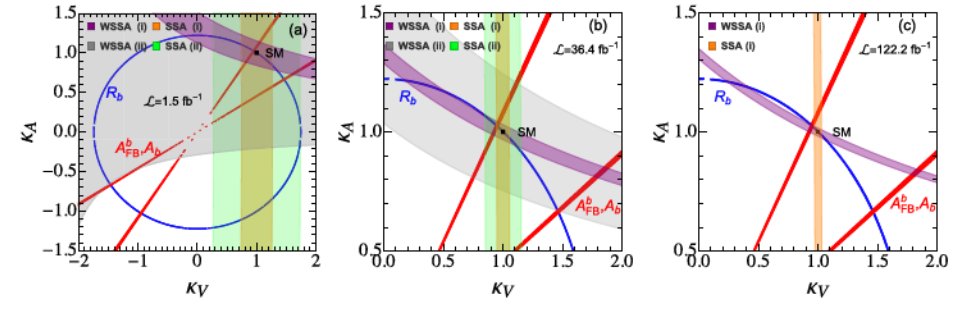


Fig. 4. The expected limits on the $Zb\bar{b}$ anomalous couplings κ_V and κ_A at the EIC with 68% C.L. The blue and red regions come from the R_b and $(A_{\rm PR}^b, A_b)$ measurements at the LEP and SLC, respectively. The purple and gray bands come from the measurements of the WSSA A_{ν}^{bQ} at the EIC with the tagging efficiency scenarios (i) and (ii), cf. Eq. (7), respectively, while the orange and green shaded regions correspond to the expected results from the SSA measurement.

and the mass of heavy quarks. As a result, the determination of the Zbb couplings from WSSA is sensitive to the b-tagging efficiency. We demonstrated that the WSSA A_e^{bQ} is sensitive to the axial-vector component of the Zbb coupling, which is in contrast to the sensitivity to the Zbb vector component from the SSA measurement and plays a complementary role on constraining the Zbb anomalous couplings. Similar to the SSA, the WSSA at the EIC could also clarify the long-standing discrepancy between the LEP A_{ER}^{b} measurement and the SM prediction owing to the high luminosity of the EIC.

Declaration of competing interest

The authors declare that they have no known competing financial interests or personal relationships that could have appeared to influence the work reported in this paper.

Acknowledgements

This work is partially supported by the U.S. Department of Energy Office of Science, Office of Nuclear Physics, under Contract DE-AC52-06NA25396 through the LANL/LDRD Program, as well as the U.S. National Science Foundation under Grant No. PHY-2013791. C.-P. Yuan is also grateful for the support from the Wu-Ki Tung endowed chair in particle physics.

References

- [1] P.A. Zyla, et al., Particle Data Group, PTEP 2020 (2020) 083C01.
- [2] D. Choudhury, T.M. Tait, C. Wagner, Phys. Rev. D 65 (2002) 053002, arXiv:hepnh/0109097
- [3] K. Agashe, R. Contino, L. Da Rold, A. Pomarol, Phys. Lett. B 641 (2006) 62, arXiv: hep-ph/0605341.
- [4] S. Gori, J. Gu, L.-T. Wang, J. High Energy Phys. 04 (2016) 062, arXiv:1508.07010.
- [5] D. Liu, J. Liu, C.E.M. Wagner, X.-P. Wang, Phys. Rev. D 97 (2018) 055021, arXiv: 1712.05802.
- [6] B. Yan, C.P. Yuan, Phys. Rev. Lett. 127 (2021) 051801, arXiv:2101.06261.
- [7] B. Yan, Z. Yu, C.P. Yuan, Phys. Lett. B 822 (2021) 136697, arXiv:2107.02134.
- [8] D. Krohn, M.D. Schwartz, T. Lin, W.J. Waalewijn, Phys. Rev. Lett. 110 (2013) 212001, arXiv:1209.2421.

- [9] W.J. Waalewijn, Phys. Rev. D 86 (2012) 094030, arXiv:1209.3019.
- [10] H.T. Li, I. Vitev, Phys. Rev. D 101 (2020) 076020, arXiv:1908.06979.
- [11] H.T. Li, I. Vitev, Phys. Rev. Lett. 126 (2021) 252001, arXiv:2010.05912.
- [12] Z.-B. Kang, X. Liu, S. Mantry, D.Y. Shao, Phys. Rev. Lett. 125 (2020) 242003, arXiv:2008 00655
- [13] Z.-B. Kang, X. Liu, S. Mantry, M.C. Spraker, T. Wilson, Phys. Rev. D 103 (2021) 074028. arXiv:2101.04304.
- [14] G. Aad, et al., ATLAS, Phys. Rev. D 93 (2016) 052003, arXiv:1509.05190.
- [15] A.M. Sirunyan, et al., CMS, J. High Energy Phys. 10 (2017) 131, arXiv:1706.
- [16] S. Moch, J.A.M. Vermaseren, A. Vogt, Nucl. Phys. B 688 (2004) 101, arXiv:hepph/0403192.
- [17] S. Catani, D. de Florian, G. Rodrigo, W. Vogelsang, Phys. Rev. Lett. 93 (2004) 152003, arXiv:hep-ph/0404240.
- [18] R.D. Field, R.P. Feynman, Nucl. Phys. B 136 (1978) 1.
- [19] C.W. Bauer, S. Fleming, D. Pirjol, I.W. Stewart, Phys. Rev. D 63 (2001) 114020, arXiv:hep-ph/0011336.
- [20] C.W. Bauer, D. Pirjol, I.W. Stewart, Phys. Rev. D 65 (2002) 054022, arXiv:hepph/0109045.
- [21] C.W. Bauer, S. Fleming, D. Pirjol, I.Z. Rothstein, I.W. Stewart, Phys. Rev. D 66 (2002) 014017, arXiv:hep-ph/0202088.
- [22] M. Beneke, A.P. Chapovsky, M. Diehl, T. Feldmann, Nucl. Phys. B 643 (2002) 431, arXiv:hep-ph/0206152.
- [23] S.D. Ellis, C.K. Vermilion, J.R. Walsh, A. Hornig, C. Lee, J. High Energy Phys. 11 (2010) 101, arXiv:1001.0014.
- [24] A. Jain, M. Procura, W.J. Waalewijn, J. High Energy Phys. 05 (2011) 035, arXiv: 1101.4953.
- [25] T. Sjostrand, S. Mrenna, P.Z. Skands, Comput. Phys. Commun. 178 (2008) 852, arXiv:0710.3820.
- [26] E. Braaten, K.-m. Cheung, S. Fleming, T.C. Yuan, Phys. Rev. D 51 (1995) 4819, arXiv:hep-ph/9409316.
- [27] M.A.G. Aivazis, F.I. Olness, W.-K. Tung, Phys. Rev. D 50 (1994) 3085, arXiv:hepph/9312318.
- [28] M.A.G. Aivazis, J.C. Collins, F.I. Olness, W.-K. Tung, Phys. Rev. D 50 (1994) 3102, arXiv:hep-ph/9312319.
- [29] J.C. Collins, Phys. Rev. D 58 (1998) 094002, arXiv:hep-ph/9806259.
- [30] M. Krämer, F.I. Olness, D.E. Soper, Phys. Rev. D 62 (2000) 096007, arXiv:hep-ph/ 0003035.
- [31] W.-K. Tung, S. Kretzer, C. Schmidt, J. Phys. G 28 (2002) 983, arXiv:hep-ph/
- [32] S. Dulat, T.-J. Hou, J. Gao, M. Guzzi, J. Huston, P. Nadolsky, J. Pumplin, C. Schmidt, D. Stump, C.P. Yuan, Phys. Rev. D 93 (2016) 033006, arXiv:1506.07443.
- [33] A. Accardi, et al., Eur. Phys. J. A 52 (2016) 268, arXiv:1212.1701.
- [34] S. Chekanov, et al., ZEUS, Eur. Phys. J. C 62 (2009) 625, arXiv:0901.2385.